Mechanical characterisation of hydrophobic and hydrophilic acrylates used in intraocular lenses through depth sensing indentation

I. Cabeza-Gil [a], B. Calvo [a,b], A. Rico [c], C. Reinhards-Hervás [c], J. Rodríguez [c,*]

[a] *Aragon Institute of Engineering Research (i3A), University of Zaragoza, Spain*
[b] *Centro de Investigacion Biomedica en Red en Bioingenieria, Biomateriales y Nanomedicina (CIBER-BBN), Spain*
[c] *Durability and Mechanical Integrity of Structural Materials, Rey Juan Carlos University, Spain*

ARTICLE INFO

ABSTRACT

In this work, the mechanical behaviour of hydrophilic and hydrophobic acrylates has been characterised by depth sensing indentation. Time-dependent behaviour has been studied using load-relaxation tests. Experiments have been simulated with a finite element software using a visco-hyperelastic material model. The parameters of this model have been determined using deep learning techniques. The developed material models have been used to mechanically simulate a standard compression test of a prototype intraocular lens.

1. Introduction

The earliest intraocular lenses (IOLs), in 1949, were made of a fairly rigid material, the polymethylmethacrylate (PMMA) (Ridley, 1952). Since then, other material alternatives have gradually emerged: hydrophilic acrylate-based hydrogels with a glass transition temperature, T_g, clearly above the operating temperature; hydrophobic acrylates with T_{gs} below the working temperature; and, finally, a family of silicone-based materials, although they have been overtaken by soft acrylates due to the risk of tearing when placing the IOL and their tendency to become opalescent (Argal, 2013). The use of foldable materials such as hydrophobic and hydrophilic acrylate polymers in IOLs have increased greatly since 1970s with the introduction of phacoemulsification and the ability to remove the cataract with smaller incisions (Amzallag and Pynson, 2007; Zvorničanin and Zvorničanin, 2018).

The excellence biocompatibility and optical clarity of acrylates, along with the ease of manufacture and implantation have made them the leading edge of IOLs to date (Kirchhof et al., 2015; Bhamra and Tighe, 2017). Even these acrylates have contributed to other ophthalmic solutions such as contact lenses (Pérez-Vives, 2018). The main difference between the two most widely used types of acrylate polymers, hydrophobic and hydrophilic, is the ability to absorb and retain water (Zvorničanin and Zvorničanin, 2018). This implies that these two acrylates behave differently when implanted within the eye, leading to different postoperative complications. Hydrophobic acrylate is associated with glistening and dysphotopsias due to its high refractive index while the main complication related to hydrophilic acrylate is the early onset of posterior capsule opacification (PCO) (Zvorničanin and Zvorničanin, 2018; Pérez-Vives, 2018).

There are few studies that intrinsically analyse the raw properties of acrylic materials. Kamata et al. (2015) (Kamata et al., 2015) evaluated the importance of swelling control on the subsequent mechanical behaviour in hydrogels. A group from Birmingham analysed the mechanical and surface properties of different hydrophilic monomers, typical of contact lenses (Kamata et al., 2015; Barnes et al., 1988; Bhamra et al., 2018). Finally, we proposed a hyperelastic model to reproduce the mechanical behaviour of IOL hydrophobic acrylate through macroscopic experimental tests under hydrated conditions (Cabeza-Gil et al., 2020, 2021a). However, in our tests we also observed a significant viscoelastic influence as reported by Bayat et al. (2020) (Bayat et al., 2020) in hydrogels, which could be key in the post-surgical biomechanical behaviour of the IOL within the capsular bag.

To our knowledge, the time-dependent mechanical behaviour of hydrophobic and hydrophilic IOL acrylates has not been characterised under dry and hydrated conditions, beyond the aforementioned studies and certain mechanical characteristics that may appear in manufacturer's catalogues (Benz Research & Development). Therefore, the objective of this study is twofold: to characterise the mechanical behaviour in dry and hydrated states of the hydrophobic and hydrophilic acrylates used in IOLs and to describe the time-dependent response. To do this, both materials were tested using spherical microindentation, as recent studies have shown the ability to reliably and

---

consistently probe the mechanical properties of materials at the microscale (Shan et al., 2007; Patel and Kalidindi, 2016; Pathak and Kalidindi, 2015; MacManus et al., 2017). A visco-hyperelastic model whose parameters has been extracted by an iterative inverse finite element algorithm (hereinafter iFEM) was used to describe the mechanical behaviour of the IOL acrylates under investigation. With this increasingly popular methodology, it is possible to bypass the manufacturing stage and numerically analyse a larger number of samples.

Due to the importance of the patient's visual quality in the post-cataract surgery period (appearance of post-operative cataract complications and the biomechanical stability of the IOL), the biomedical performance of IOL acrylates is of enormous relevance. There are several investigations looking at post-cataract complications related to IOL materials, such as in-vivo PCO (Findl et al., 2010; Chang and Kugelberg, 2016) and glistenings (Pagnoulle et al., 2012; Tetz and Jorgensen, 2015). A combination of both materials, hydrophobic and hydrophilic acrylate, has even been made using interpenetrating photopolymers to avoid such complications (Shaik et al., 2016). To introduce a new IOL to the market, mechanical stability must be analysed, following the standard compression test ISO 11979–3 (Cabeza-Gil et al., 2020; Cabeza-Gil et al., 2021a; BS EN ISO 11979–3:2012, 2012). This test is usually carried out experimentally, however, it is also possible to carry it out numerically, with the advantage of reducing both time and costs (Cabeza-Gil et al., 2020; Bozukova Dand Werner et al., 2015; Remón et al., 2018). To obtain accurate results, it is essential to have a proper characterisation of the behaviour of the IOL material. Therefore, in addition to characterising the hydrophobic and hydrophilic material used in IOLs, the standard IOL compression test (BS EN ISO 11979–3:2012, 2012) was simulated with the proposed material models to show a possible application of the analyses performed here.

2. Materials & methods

2.1. Materials

Two different materials have been selected: hydrophobic acrylic material Benz HF-1.2 Universal Blank (Benz Research and Development, USA) and hydrophilic acrylic material Benz IOL 25 (Benz Research & Development, USA) (Benz Research & Development). Hydrophilic acrylate has a greater tendency to hydrate (30 wt%) compared to hydrophobic acrylate (<5 wt%). Both materials have been characterised in two different conditions: hydrated to equilibrium and dry. Dry cylindrical specimens of 2.56 mm and 2.19 mm in height, and 15.22 mm and 12.75 mm in diameter have been used for hydrophilic and hydrophobic acrylate, respectively. To achieve hydration, specimens were immersed in 0.9% Vitulia physiological serum for a period of 48 h to guarantee the balance of the systems. This time is much longer than that required to achieve maximum hydration, which has been experimentally determined at 20 min for hydrophobic acrylate and at 24 h for hydrophilic acrylate.

2.2. Spherical indentations

Load–relaxation microindentation tests were carried out using an Agilent G200 nanoindenter equipped with a Keysigth XP indentation head and a 500 mN load cell. All the tests were performed at a controlled temperature of 20 °C using an 800 μm ruby spherical tip. Three batches of load-relaxation tests have been completed maintaining the penetration distance for a holding time of 1500 s for each material. The hydrated samples have been tested in a sample holder that allows them to be kept submerged in 0.9% physiological saline during the tests. In this way, constant hydration conditions are guaranteed. Table 1 shows the most important parameters used to perform the tests.

Table 1
Tests parameters.

Material	Condition	Holding Penetration Distance	Holding Time	Loading Rate	Drift Rate
(–)	(–)	(μm)	(s)	(s^{-1})	(nm/s)
Hydrophilic acrylate	Dry	2.5	>1500	0.006	<0.05
		5			
		7.5		0.004	
	Hydrated	10		0.033	<1
		15			
		20			
Hydrophobic acrylate	Dry	10		0.011	<0.05
		15			
		20			
	Hydrated	15		0.011	<1
		20			
		25			

2.3. Computational finite element model

The microindentation experiments were simulated by developing a 2D axisymmetric finite element (FE) model using the Abaqus software, see Fig. 1. Large strain and non-linear features were adopted in this dynamic simulation. It is assumed that a spherical indenter tip is pressed into a cylinder of material that should be representative of a homogenous infinite half space. The diamond spherical indenter tip was modelled as a rigid material and its loading was prescribed as an applied displacement coincident with that of the experiments. The specimen is assumed to be a deformable solid and is characterised by an incompressible visco-hyperelastic Neo-Hookean material model, which is described in Eq. (1):

$$\psi(\mathbf{C}, t) = C_{10}^R(t)\,(I_1 - 3) \tag{1}$$

Being $\psi(\mathbf{C}, t)$ the strain energy density function, $C_{10}^R(t)$ the hyperelastic Neo-Hookean constant and I_1 the first invariant of the right Cauchy-Green deformation tensor, $\mathbf{C}$. The time dependence of $C_{10}^R(t)$ is defined by a two term ($N = 2$) Prony series:
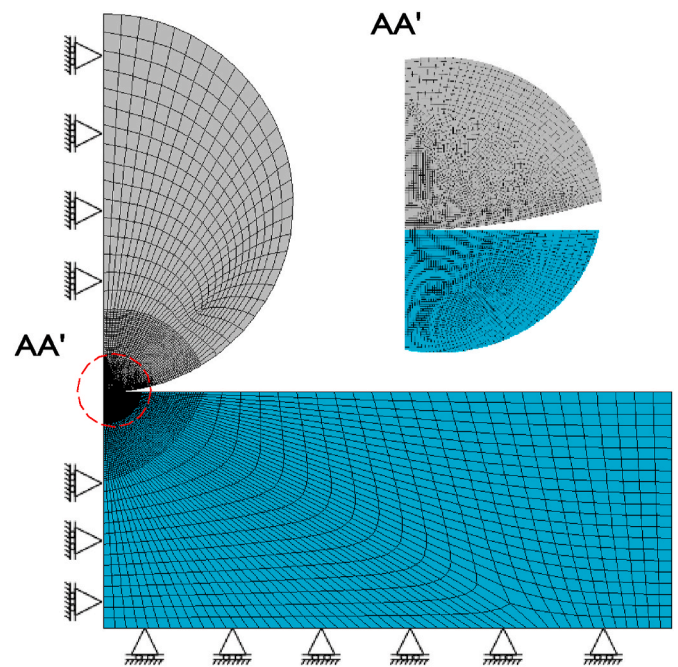
Fig. 1. FE model used to simulate the microindentation experiments. The material specimen (blue) was meshed with 4563 CAX4H elements whilst the spherical indenter (grey) was meshed with 3333 CAX4 elements.

$$C_{10}^{R}(t) = C_{10}^{0} \left(1 - \sum_{i=1}^{N} g_i \left(1 - e^{-\frac{t}{\tau_i}} \right). \right) \tag{2}$$

$$C_{10}^{\infty} = C_{10}^{0} \left(1 - \sum_{i=1}^{N} g_i \right) \tag{3}$$

Being $\mathbf{C}_{10}^{0}$, the instantaneous modulus and C_{10}^{∞}, the long-term modulus, defined in Eq. (2) and (3). The Prony series parameters are defined by the pre-exponential factors g_i and the relaxation times τ_i.

For consistency with linear elasticity in small deformations, the incompressible Neo-Hookean model can be converted to a linear elastic model with the following relationship:

$$\mu = 2C_{10}, \quad E = 3\mu \tag{4}$$

Being μ the first Lamé parameter, and E, the Young' modulus.

A four-node quadrilateral hybrid element (CAX4H) was used to mesh the indenter and the specimen using a finer mesh in the region where the two bodies are expected to be in contact. The size of the elements is 4 μm for the indenter and the specimen in the area of interest, see Fig. 1. Surface-to-surface contact definition was used to avoid any accumulation of concentrated force on the individual nodes at the initial point of contact, and the 'hard' contact approach, that uses the direct method as constraint contact method, was considered to minimise penetration between the slave and master surfaces. The direct method strictly enforces a given pressure-overclosure behaviour for each constraint, without approximation or use of augmentation iterations.

2.4. iFEM optimisation

To adjust the visco-hyperelastic response of the materials analysed, a two-step inverse methodology was proposed. First, the long-term modulus of the hyperelastic contribution of the material was obtained. For this, it is assumed that the load at the end of each experimental test (t = 1500 s) only had a hyperelastic contribution, that is, the viscoelastic relaxation has previously occurred. As a result, we had the load relaxation curves associated with the three experimental tests performed at three different holding penetration distances. To compare the experimental and numerical results, the error considered was the normalized mean absolute error (nMSE). To find the optimal hyperelastic parameter (C_{10}^{∞}) of the Neo-Hookean model proposed, a batch of 20 simulations was initially performed. The hyperelastic parameter (C_{10}^{∞}) of this batch of simulations was calculated based on a theoretical approach (Cabeza-Gil et al., 2020; Syngellakis et al., 2017). Then, the inverse finite element iterative algorithm (iFEM) sought the optimal parameter that minimised the error (nMSE) through a process of optimisation of the simulation database. If no case was deemed suitable (*error* > *Tol*$_{max}$), a deep neural network (DNN) fed by the database, calculated the optimal material parameter which minimised the error. A new simulation was submitted with this calculated material coefficient and added to the database. This process was repeated until the imposed tolerance was accomplished, see Fig. 2. The implemented DNN was based on the work of Papazafeiropoulos et al. (2017) (Papazafeiropoulos et al., 2017) to calculate the optimal cohesive and friction coefficients. The time required by iFEM to fit material properties was highly dependent on the first batch of simulations submitted.

Second, the same procedure was followed to fit the Prony series parameters. In this case, a dynamic simulation was performed that exactly replicates the experimental test conditions. The database was generated from 300 simulations for each loading displacement in each material, resulting in 900 simulations. Contrary to the fitting of the hyperelastic material properties, the use of DNN is key in this procedure due to the high non-linearity related to the four adjusted Prony parameters (g_1, g_2, τ_1 and τ_2). In this case, six points were experimentally and numerically compared: for each holding penetration distance, the maximum load applied by the indenter (t = 90 s for hydrophobic materials) and the load applied at t = 140 s. The implemented methodology is summarised in Fig. 2.

3. Results and discussion

The resulting displacement obtained from the microindentation experiments is shown in Fig. 3, as proof of the adequate execution of the tests with excellent indenter control. After an initial ramp with the strain
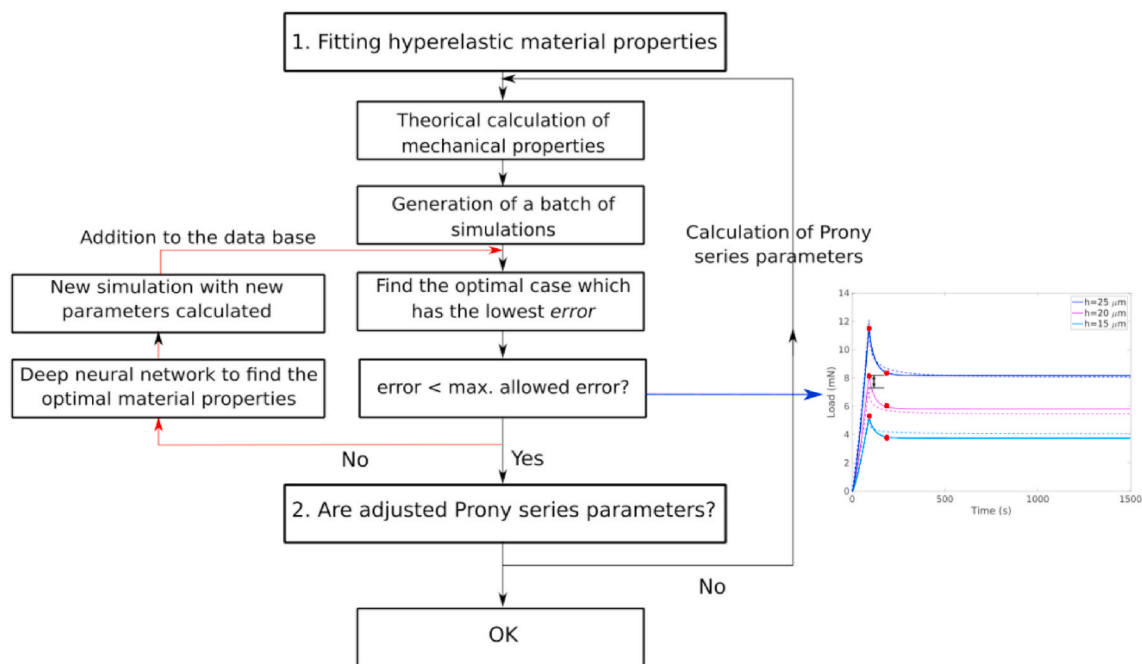

Fig. 2. Outline of the inverse methodology to find the optimal Prony series parameters. An example of the six points used to calculate the error and fit the DNN is shown on the right (red points). Each individual error was calculated as the absolute difference between the experimental and numerical data. The error used to fit the DNN was calculated as the average normalized mean of the six points compared.
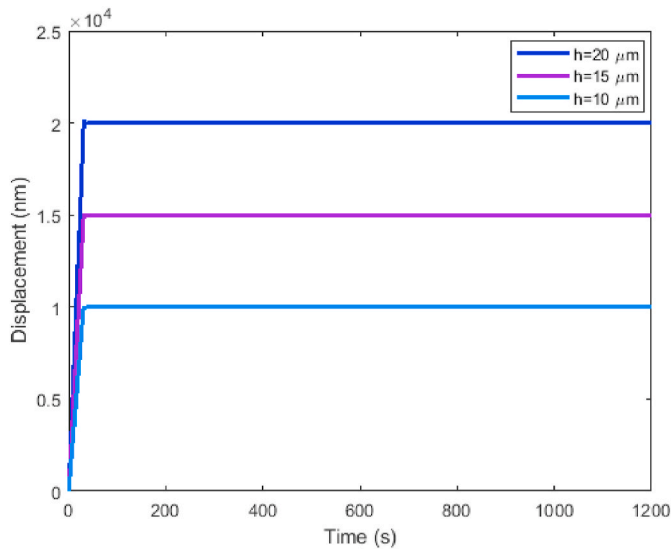
Fig. 3. Example of displacement control for experimental relaxation corresponding to the hydrophilic material tested. at hydrated conditions.

rate prescribed in Table 1, a holding penetration distance was kept during more than 1500 s.

3.1. Calibration of the visco-hyperelastic material model

Fig. 4 shows the experimental and numerical data of the tests performed for the three holding penetration distances, see Table 1, on each acrylate material in both states, hydrated and dry. The visco-hyperelastic coefficients obtained after performing the iFEM optimisation are presented in Table 2. All numerical values were within the deviation measured in the experimental tests, and the average nMAE of the three holding penetration distances was always below 0.02. The

response surface methodology is the one commonly used in parameter fitting problems. On the contrary, in this case the iFEM optimisation has been used to adjust the visco-hyperelastic coefficients (Papazafeiropoulos et al., 2017), which allowed reducing computational costs. The presented methodology could be more useful in highly non-linear approaches.

It should be noted that the load response presents a time-dependence for all materials regardless their degree of hydration. It can be seen that the time-dependent trends seem to find a horizontal asymptote within the test time. There is also, as expected, a perfect correlation between greater penetration distances and higher loads. In all the samples tested, lower loads are observed when they are in the hydrated condition compared to the dry samples of the same material. This decrease in stiffness is a consequence of introducing serum inside, an obviously more pronounced behaviour in hydrophilic acrylate due to its much higher water absorption capacity.

The results and the parameters obtained show the different behaviour between the hydrophobic and hydrophilic acrylate. While the mechanical properties of the hydrophobic acrylate change slightly in the state of hydration, the properties of the hydrophilic change completely according to its state. This is due to its Tg, which is several tens above the working temperature.

An estimation of the long-term Young' modulus was performed considering the consistency with linear elasticity of Neo-Hookean hyperelastic model of an incompressible material, see Eq. (4). The values obtained, see Table 2, are consistent with the values reported in literature (Bhamra et al., 2018; Cabeza-Gil et al., 2020) and with the manufacturer's catalogs (Benz Research & Development). The numerical fitting showed that the hydrated hydrophilic acrylate is the most flexible material, followed by the hydrated and dry hydrophobic acrylate. The dry hydrophilic acrylate is significantly stiffer than the materials mentioned above. For the same holding penetration distance of 15 µm, the hydrated hydrophilic acrylate presented a maximum load of 3.76 ± 0.26 mN while the hydrated and dry hydrophobic acrylate presented a maximum load of 5.06 ± 0.14 mN and 8.21 ± 0.33 mN,
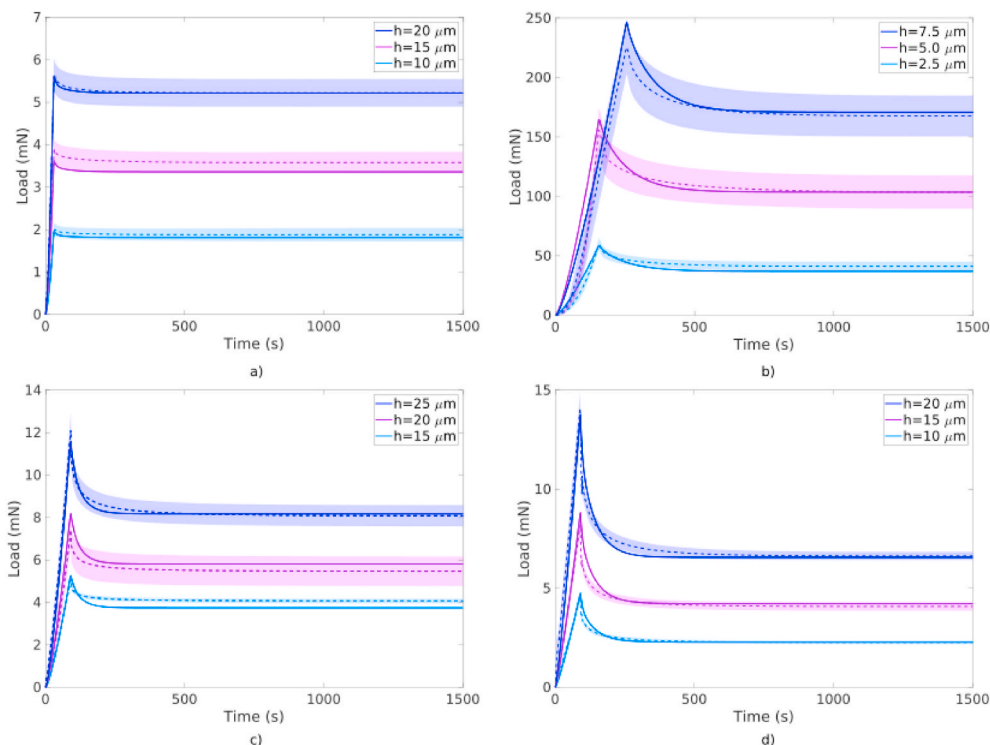

Fig. 4. Experimental (mean (dashed line) and standard deviation) and numerical (continuous line) loads vs. time. a) Hydrophilic tested at hydrated conditions. b) Hydrophilic tested at dry conditions. c) Hydrophobic tested at hydrated conditions. d) Hydrophobic tested at dry conditions.

Table 2
Viscohyperelastic parameters for the materials adjusted in the spherical indentation tests.

Acrylate	State	Hyperelastic contribution		Viscohyperelastic contribution			
		C_{10}^{∞} (MPa)	E (MPa) (Eq. (4))	g_1 (−)	g_2 (−)	τ_1 (s)	τ_2 (s)
Hydrophilic	hydrated	0.18	1.08	0.11	0.04	11.30	57.25
Hydrophilic	Dry	33.88	203.30	0.39	0.20	88.01	10.00
Hydrophobic	hydrated	0.21	1.26	0.30	0.26	15.04	39.12
Hydrophobic	Dry	0.24	1.44	0.64	0.21	5.16	48.80

respectively. The same trend was obtained analysing the experimental force exerted in IOL delivery (Cabeza-Gil et al., 2021b). This additional stiffness in the dry material could involve some risk factors such as damaging in IOL delivery. Considering the importance of using soft materials in delivery and placement, IOLs should always be in their hydrated state prior to be injected in the eye (Cabeza-Gil et al., 2021b).

3.2. Theoretical calculation of linear modulus

In a linear elastic material, a spherical indentation is described by the following relationship between the applied load, *P*, and the depth of penetration, *h*:

$$P = \frac{4}{3}R^{1/2}h^{3/2}\frac{E}{1 - v^2} \tag{5}$$

where *R* is the indenter radius, *E* the elastic modulus and ν the Poisson's ratio. Zhang et al. (2014) (Zhang et al., 2014) extended this expression to non-linear elastic behaviour, introducing correction terms calculated from finite element simulations. In the case of a Neo-Hookean model, Eq. (5) is modified by a factor that depends on the relative penetration:

$$P = \frac{4}{3}R^{1/2}h^{3/2}\frac{E}{1 - v^2}\left(1 - 0.15\frac{h}{R}\right) \tag{6}$$

For small penetration depths, the correction included in Eq. (6) is negligible. In the case of a viscoelastic material, the elastic modulus is substituted by the relaxation function *E(t)*. Poisson's ratio is usually assumed to be constant, for the sake of simplicity. Fig. 5 shows the value of *E(t)* for the hydrophobic and hydrophilic acrylates both in dry and hydrated conditions.

As can be seen, hydrophilic acrylate hardly shows relaxation when it acts in hydration, being a very good approximation to consider it as an eminently elastic material. The response in dry conditions is very different showing a strong viscoelastic character. However, this matter is of no practical interest since the material is not used under these conditions. Regarding to hydrophobic acrylate, the material shows a marked relaxation close to 20% and although, as already mentioned, it presents stiffness values similar to those of hydrophilic, the response to relaxation constitutes an important difference between both materials. The elastic modulus calculated with the theoretical approach were similar to those calculated numerically with the finite element method, see Table 2.

3.3. Linear time-dependent behaviour

The time-dependent response can be characterised assuming a linear viscoelastic behaviour. The relaxation function can be written as a Prony
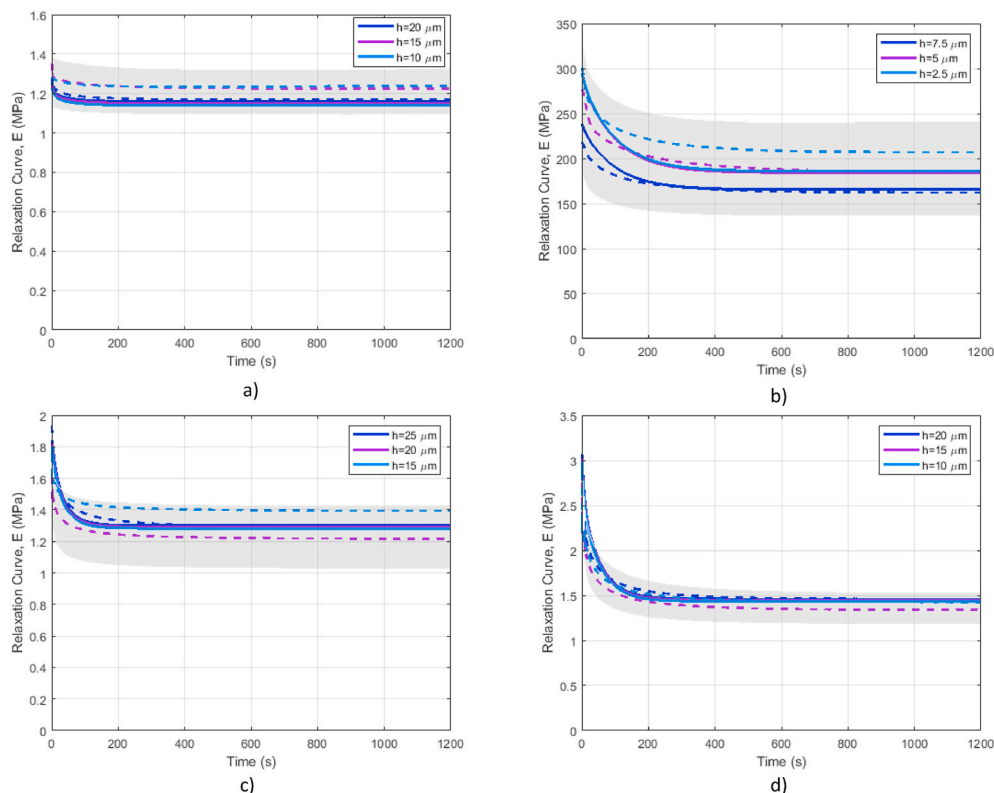
Fig. 5. Experimental (solid lines) and numerical (dashed lines) relaxation curves. a) Hydrophilic tested at hydrated conditions. b) Hydrophilic tested at dry conditions. c) Hydrophobic tested at hydrated conditions. b) Hydrophobic tested at dry conditions. Grey zone includes the experimental absolute error.

series by Eq. (7).

$$E(t) = E_\infty + (E_0 - E_\infty) \left(\sum_{i=1}^{n} A_i e^{-\frac{t}{\tau_i}} \right) \tag{7}$$

where E_0 and E_∞ are the instantaneous and long-term value of the relaxation function, τ_i the relaxation time of the i-term of the Prony series with the pre-exponential factor A_i. The experimental loads in the spherical indentation tests can be normalized by using Eq. (8).

$$\frac{P(t) - P_\infty}{P_0 - P_\infty} = \frac{E(t) - E_\infty}{E_0 - E_\infty} = \left(\sum_{i=1}^{n} A_i e^{-\frac{t}{\tau_i}} \right) \tag{8}$$

Using the above equation allows you to cancel out differences in stiffness and focus on relaxation in relative terms. In a primarily viscoelastic material, the indentation curves corresponding to different penetration depths should collapse in a single curve. As it can be observed in Fig. 6, this is precisely the case for the materials under investigation, despite the experimental uncertainty. Especially in the hydrophobic material that responds perfectly to what a viscoelastic material should do (experimental curves at different penetrations merge into a single curve in a practically ideal way). Fig. 5 and 6 together give us an idea of the behaviour of the materials used in IOLs, always in hydrated conditions. The results indicate that the stiffness of the hydrophobic and hydrophilic materials is similar, but hydrophobic acrylate appears to have a more marked time-dependent behaviour, with clearly greater absolute relaxation. The clinical importance of this aspect should be analysed but it is outside the scope of this work. In any case, the experimental results are consistent with the use of viscoelastic models to describe these materials. This is the main result of this work, in which the hydrophobic and hydrophilic acrylates have been adjusted to a hyperelastic-linear viscoelastic FE model, which reasonably describes the experiments as indicated in Fig. 5. The specific values of the parameters after the simulation optimisation process have been included in Table 2.

3.4. Discussion about the contact model in terms of adhesion

As was previously stated, experimental curves have been mainly interpreted in terms of a Hertz - type contact model, although hyperelastic and viscoelastic modifications have been introduced in both the theoretical and numerical models. It is worthy to note that several hypothesis are linked to this model. Particularly, adhesion between material and indenter should be carefully treated, because Hertz theory framework does not take into account this type of interaction. Note that in soft and sticky materials, adhesion could be a relevant phenomenon that has to be considered if adhesion level is high enough to show relative importance on the experimental forces that are measured during the relaxation experiments.
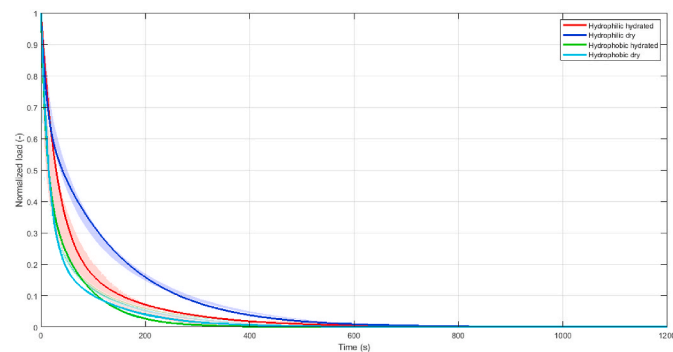
Several models have been developed to include the adhesion in contact mechanics (Popov et al., 2019; Borodich, 2014). The aplicability of these models is determined by the so - called Tabor parameter, which scales the extension of the adhesion area between indenter and sample. Several authors have claimed (Ciavarella et al., 2019) that a normalized load can be included to determine exactly the adhesion regime describing a particular indenter/sample system. Moreover, indenter radius and contact radius stablished between sample and indenter also play a role in determining the adhesion regime that characterises a particular experimental situation. An adhesion map (Ciavarella et al., 2019) can be consulted in terms of the normalized load and the Tabor parameter. The normalized load is computed as:

$$\widehat{P} = \frac{P}{\pi R \omega} \tag{9}$$

where ω is the work of adhesion per unit area, P is the load imposed during the experiment and R is the indenter radius. To obtain the value of the normalized load it is necessary to known ω, that can be computed from the initial stage of the loading branch of the indentation tests. In Fig. 7, loading curves from hydrated hydrophilic and hydrophobic acrylates are shown. A detail of the starting part of the loading trend is also
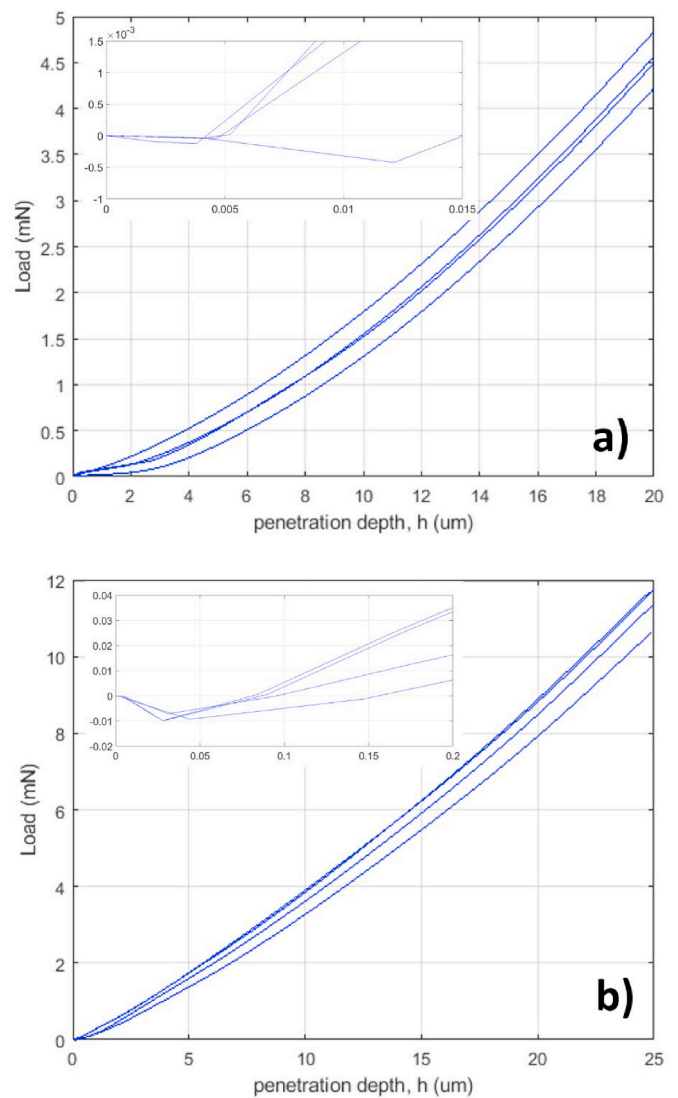
Fig. 6. Time-depended response: normalized load vs. time. Shaded zones correspond to experimental variability and solid lines are the numerical outputs.

Fig. 7. Load vs. displacement curve. Detail of the initial part of the loading curve are included as an inserts in figures. a) Hydrophilic acrylate. b) Hydrophobic acrylate.

depicted.

Negative values of the compression force, i.e., tension values, are observed for the low penetration depth regime. This a sign of adhesion between sample and indenter. The maximum force in the adhesion loop, Fc, can be used to estimate the adhesion work per unit area. Following the Johnson – Kendal – Roberts adhesion theory and taking into account that the tests are performed under displacement control, ω can be computed as:

$$\omega = \frac{6}{5}\frac{Fc}{\pi R} \tag{10}$$

In Table 3 maximum adhesion forces, Fc, and work of adhesion derived using Eq. (10) are collected for both materials under hydrated conditions for all experimental tests. The work of adhesion is much lower for hydrophilic material than for hydrophobic acrylate and, although adhesion should be measured for the particular system between materials in contact, these values are in the same order of magnitude than others previously measured in similar materials (Lombardo et al., 2009). Using Eq. (9), the normalized load can be determined for the maximum load reached for each sample during the relaxation test (5 mN and 12 mN for hydrophilic and hydrophobic materials, respectively, see Fig. 4). The normalized load reaches values of 6600 and 720 for hydrophilic and hydrophobic materials, respectively. If these values are translated to the adhesion map in (Ciavarella et al., 2019), it is clear that only two models for the mechanics of this particular contact are valid. For low or intermediate values of Tabor parameter, Hertz model describes the particular contact under the experimental conditions. However, if Tabor parameter is relatively high, Johnson – Kendal – Roberts adhesion theory becomes a better description of the contact mechanics for this situation (Johnson et al., 1971). This justifies the use of Eq. (10) for calculating the work of adhesion.

When non-adhesive indentation experiments are performed, the effective elastic modulus E* (or the indentation relaxation function for viscoelastic materials) is usually estimated using the contact stiffness, S, which is the slope the P − h curve at the unloading branch. Using Hertz model, contact stiffness can be calculated taking the derivative of the load over the displacement in Eq. (5), resulting in:

$$S = \frac{dP}{dh} = 2E^*a \tag{11}$$

where a is the contact radius (equal to $\sqrt{Rh}$). However, due to adhesive effects Eq. (11) should be modified using a JKR approach:

$$S = 2E^*af \tag{12}$$

where f is a correction factor depending on the work of adhesion per unit area, the effective modulus and the contact radius, following Borodich et al. (2021) (Borodich et al., 2021):

Table 3
Experimental adhesion load and adhesion work for hydrophilic and hydrophobic acrylates tests.

Material	Radius	Max Penetration	Adhesion Load	Adhesion work
(−)	(μm)	(μm)	(mN)	(J/m2)
Hydrophilic Acrylate	800	20	−0,00042	0,00020
			−0,00005	0,00002
			−0,00004	0,00002
			−0,00010	0,00005
		Average	**−0,00015**	**0,00007**
		Std. Desv.	**0,00005**	**0,00002**
Hydrophobic Acrylate		25	−0,010	0,0048
			−0,009	0,0045
			−0,010	0,0047
			−0,007	0,0034
		Average	**−0,009**	**0004**
		Std. Desv.	**0,001**	**0001**

$$f = \frac{1 - 3\sqrt{\frac{\pi R^2 \omega}{8E^* a^3}}}{1 - \sqrt{\frac{\pi R^2 \omega}{8E^* a^3}}} \tag{13}$$

The f factor can be used as a criterion to establish if Hertz – type models are suitable for use. If the factor f is close to one (for example if work of adhesion is low in relation to the material stiffness) then, it is not necessary to take adhesion into account for calculations and Eq. (11) can be used by committing a low error. Note that f factor needs the modulus and contact radius to be determined in advance. The contact radius can be obtained using the JKR expression relating contact radius and penetration depth in Eq. (14):

$$h = \frac{a^2}{R} - \sqrt{\frac{2\pi a \omega}{E^*}} \tag{14}$$

Penetration depth is continuously measured during the loading branch of the relaxation test, and it is set at a constant value in the relaxation part of the experiment (see Fig. 3). If effective modulus is known, by solving Eq. (14), contact radius can be determined for the entire experimental test.

However, due to the viscous nature of the materials involved, f factor could change during the relaxation of the sample, leading to an evolution of the adhesion effect during the test. As the work of adhesion has been measured for hydrated materials, f factor can be computed for different values of the effective modulus. Fig. 8, shows the variation of the f factor with the penetration depth for hydrophilic and hydrophobic materials. Shaded areas corresponds to f factor computed for effective moduli ranging from 0.5 MPa (dashed lines) to 3 MPa (solid lines), covering the values that have been reported for relaxation functions in previous sections for both materials. The f factor is higher than 0.92 in the worst experimental conditions, corresponding to the hydrophobic material tested at the lower penetration depth (15 μm). The hydrophilic material shows an f factor higher than 0.95 for all cases due to the low work of adhesion that has been measured for this material.

According to these values, adhesion had a minor importance during the relaxation tests performed in this work. The use of an indenter of high radius (800 μm) and the range of experimental penetration depths, in addition to the low values of the work of adhesion measured, lead to contact conditions in which the Hertz – type models are reasonably applicable. Last, note that highest errors that have been computed are lower than the intrinsic experimental dispersion presented as shaded areas in Fig. 5.
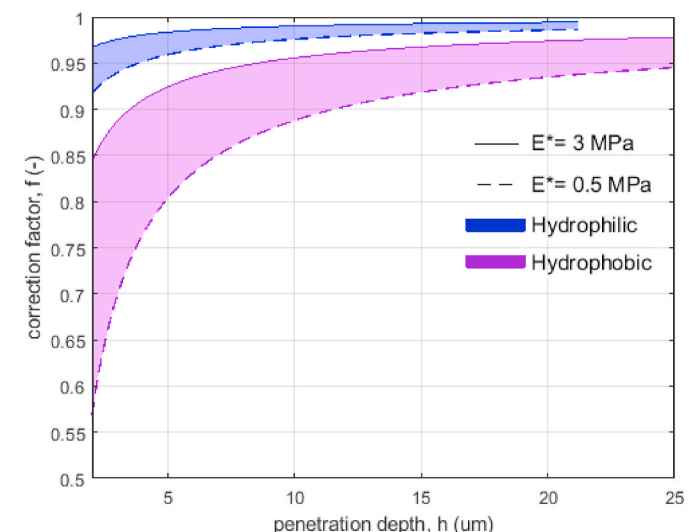

Fig. 8. f factor variation in terms on the penetration depth.

3.5. IOL compression standard test

To illustrate a case of application of the proposed material models, an IOL prototype (model #C in Cabeza -Gil et al. (2021) (Cabeza-Gil et al., 2021a)) was tested following the Standard ISO 11979–3:2012 (BS EN ISO 11979–3:2012, 2012). The IOL was compressed between two clamps from a compression diameter of 13 mm up to 10 mm in 90 s and kept the strain applied during 1500 s, see Fig. 9 (for graphical purposes the graph is only up to 600 s). To simulate the working condition, the IOL was modelled using the parameters determined for the hydrophobic and hydrophilic acrylates in hydrated condition.

The compression force was registered as the average of the two clamps, considered as rigid solids, throughout the dynamic simulation. The hydrophobic and hydrophilic IOL showed a relaxation similar to that of the microindentation tests, 35.03%, and 5.00%, respectively. Both models of IOL material presented adequate biomechanical stability (without axial displacement, tilt or rotation) in a compression diameter of 10 mm as seen in Remón et al. (2018) (Remón et al., 2018), providing quality optical performance in a hypothetical implantation.

4. Conclusions

In this work, the time-dependent mechanical behaviour of two acrylates used in the manufacture of IOLs (hydrophobic acrylic material, Benz HF-1.2 Universal Blank, Benz Research and Development USA; and hydrophilic acrylic material, Benz IOL 25, Benz Research and Development, USA) has been described through a numerical model fitted using spherical indentation relaxation tests carried out on dry and hydrated materials. The following conclusions can be drawn:

- A hyperelastic-viscoelastic model has been used to describe the behaviour of the material. The hyperelastic part captures the material non-linearity while the linear viscoelastic contribution accounts for the time-dependence of the elastic constants. The proposed material models describe relaxation tests within the experimental variability and can be used, as shown in Fig. 9, in the IOL design stage.
- The fitting procedure in the numerical model followed an optimisation process based on deep learning techniques, which represents a saving of computational time compared to other methodologies such as the response surface methodology, in addition to ensuring good agreement with the experimental results.
- Under hydrated conditions, where IOLs materials really work, the stiffnesses of hydrophobic and hydrophilic acrylates are quite similar, although the hydrophobic material is 17% stiffer. However, if the hydrophobic material is implanted in dry conditions, there is an increase in its stiffness (33% compared to the hydrated hydrophilic) that could discourage its use in clinical practice. The elastic constants corresponding to dry hydrophilic acrylate are much higher than the rest, but this is not significant due to its inappropriate use under these conditions.
- Hydrophobic acrylate shows a more pronounced time-dependent behaviour than hydrophilic one, having a higher degree of relaxation in absolute terms. Furthermore, the time dependence of the mechanical properties of the hydrophobic acrylate studied in this work is adequately described with a linear viscoelastic model. Interestingly, the normalized load versus time curve follows the same path regardless of whether the material is hydrated or dry. This is a substantial difference from the hydrophilic acrylate.
- Although adhesion effects may become important in this type of materials, it has been found that the relative influence in the experiments carried out in this work is low as a consequence of a combination of favorable experimental conditions, which justifies the use of Hertzian contact models.
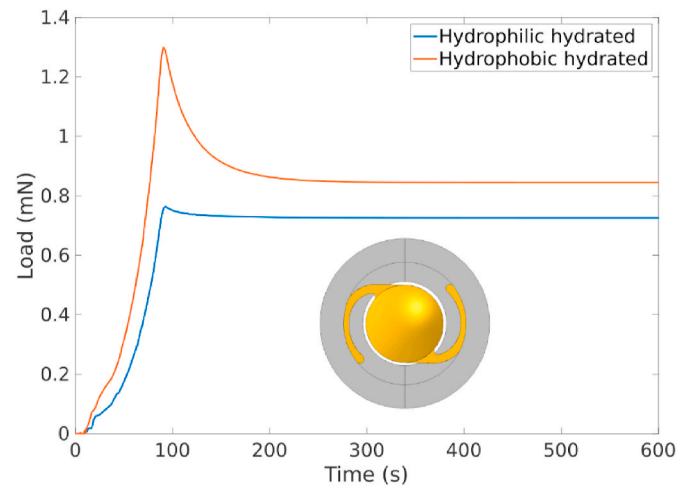

Fig. 9. Compression force of the hydrophobic and hydrophilic model #C in the standards compression tests. The FE model of the standard test can be seen in Remón et al. (2018) (Remón et al., 2018).

CRediT authorship contribution statement

I. Cabeza-Gil: Writing – original draft, Methodology, Investigation, Conceptualization. **B. Calvo:** Writing – review & editing, Conceptualization, Funding acquisition, Methodology. **A. Rico:** Conceptualization, Formal analysis, Methodology, Writing – review & editing. **C. Reinhards-Hervás:** Writing – original draft, Methodology, Investigation, Conceptualization. **J. Rodríguez:** Writing – review & editing, Methodology, Funding acquisition, Conceptualization.

Declaration of competing interest

The authors declare that they have no known competing financial interests or personal relationships that could have appeared to influence the work reported in this paper.

References

Amzallag, T., Pynson, J., 2007. J. Fr. Ophtalmol. 30, 757–767.

Argal, S., 2013. J. Clin. Ophthalmol. Res. 1, 113.

Barnes, A., Corkhill, P.H., Tighe, B.J., 1988. Polymer 29, 2191–2202.

Bayat, M.R., Wang, K., Baghani, M., 2020. Int. J. Eng. Sci. 152, 103294.

Benz Research & Development, (n.d.).

Bhamra, T.S., Tighe, B.J., 2017. Contact Lens Anterior Eye 40, 70–81.

Bhamra, T.S., Tighe, B.J., Li, J., 2018. J. Biomed. Mater. Res. B Appl. Biomater. 107, 1645–1653.

Borodich, F.M., 2014. Adv. Appl. Mech. 47, 225–366.

Borodich, F.M., Galanov, B.A., Keer, L.M., Suarez-Alvarez, M.M., 2021. Phil. Trans. Math. Phys. Eng. Sci. 379, 20200289.

Bozukova Dand Werner, L., Mamalis, N., Gobin, L., Pagnoulle, C., Floyd, A., Liu, E., Stallings, S., Morris, C., 2015. J. Cataract Refract. Surg. 41, 1490–1502.

BS EN ISO 11979-3:2012, 2012. Ophthalmic Implants. Intraocular Lenses. Mechanical Properties and Test Methods. BSI Standards Limited.

Cabeza-Gil, I., Ariza-Gracia, M.Á., Remón, L., Calvo, B., 2020. Ann. Biomed. Eng. 48.

Cabeza-Gil, I., Pérez-Gracia, J., Remón, L., Calvo, B., 2021a. J. Mech. Behav. Biomed. Mater. 114, 104165.

Cabeza-Gil, I., Ríos-Ruiz, I., Calvo, B., 2021b. J. Mech. Behav. Biomed. Mater. 124.

Chang, A., Kugelberg, M., 2016. Eur. J. Ophthalmol. 27, 164–168.

Ciavarella, M., Joe, J., Papangelo, A., Barber, J.R., 2019. J. R. Soc. Interface 16, 20180738.

Findl, O., Buehl, W., Bauer, P., Sycha, T., 2010. Cochrane Database of Systematic Reviews.

Johnson, K.L., Kendall, K., Roberts, A.D., 1971. Proc. Roy. Soc. Lond. Math. Phys. Sci. 324, 301–313.

Kamata, H., Li, X., Chung, U., Sakai, T., 2015. Adv. Healthc. Mater. 4, 2360–2374.

Kirchhof, S., Goepferich, A.M., Brandl, F.P., 2015. Eur. J. Pharm. Biopharm. 95, 227–238.

Lombardo, M., Carbone, G., Lombardo, G., De Santo, M.P., Barberi, R., 2009. J. Cataract Refract. Surg. 35, 1266–1272.

MacManus, D.B., Pierrat, B., Murphy, J.G., Gilchrist, M.D., 2017. Acta Biomater. 48.

Pagnoulle, C., Bozukova, D., Gobin, L., Bertrand, V., Pauw, M.-C.G.-D., 2012. J. Cataract Refract. Surg. 38, 1271–1277.

Papazafeiropoulos, G., Muñiz-Calvente, M., Mart\'{\i}nez-Pañeda, E., 2017. Adv. Eng. Software 105, 9–16.

Patel, D.K., Kalidindi, S.R., 2016. Acta Mater. 112, 295–302.

Pathak, S., Kalidindi, S.R., 2015. Mater. Sci. Eng. R Rep. 91, 1–36.

Pérez-Vives, C., 2018, 2018 J. Ophthalmol. 1–17.

Popov, V.L., Heß, M., Willert, E., 2019. Springer, Berlín, ISBN 978-3-662-58708-9. https://doi.org/10.1007/978-3-662-58709-6.

Remón, L., Siedlecki, D., Cabeza-Gil, I., Calvo, B., 2018. J. Biomed. Opt. 23, 1.

Ridley, H., 1952. Br. J. Ophthalmol. 36, 113–122.

Shaik, S.H., Donempudi, S., Tammishetti, S., Garikapati, K.R., Bhadra, M.P., 2016. J. Appl. Polym. Sci. 134.

Shan, Z.W., Mishra, R.K., Asif, S.A.S., Warren, O.L., Minor, A.M., 2007. Nat. Mater. 7, 115–119.

Syngellakis, S., Habbab, H., Mellor, B.G., 2017. Int. J. Comput. Methods. Exp. Meas. 6, 749–763.

Tetz, M., Jorgensen, M.R., 2015. Curr. Eye Res. 40, 969–981.

Zhang, M.G., Cao, Y.P., Li, G.Y., Feng, X.Q., 2014. Biomech. Model. Mechanobiol. 13.

Zvorničanin, J., Zvorničanin, E., 2018. J. Curr. Ophthalmol. 30, 287–296.